CHAPTER 1

Introduction of Topological Materials

1.1 Introduction

Materials are typically categorized in insulators, semiconductors, and metals based on their electronic properties. Figure 1.1 demonstrates the schematics of electronic bands in semiconductor, insulator, metal and Topological Insulators. In condensed matter physics, the energy band theory successfully explains the phenomena in semiconductors, which was unsolved to till 1930s. Since 1970s, physicists proposed a new kind of phase theory like Kosterlitz–Thouless (KT) phase transition[1], [2], Haldane phase[3], [4], quantum Hall states [5]–[9] which were different from the well-established Landau Fermi liquid theory and Landau Ginzburg Wilson theory of phase transitions and spontaneous symmetry breaking in a sense that they possess non-Fermi liquid behaviour and symmetry protection. This advanced phase theory paved the way

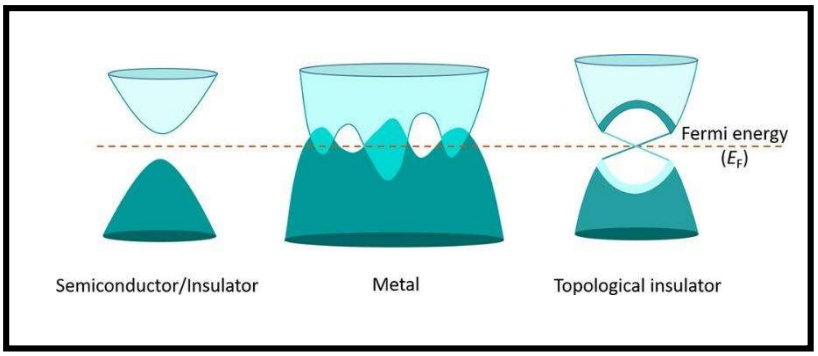

Figure 1.1 Schematics of electronic bands in various solid-state materials. In semiconductors/insulators, the valence and conduction bands are separated by an energy gap. In metals, the valence and conduction bands overlap each other. In topological insulators, after band inversion, the valence and conduction bands are separated by the band gap, leaving behind conducting topological surface states in the form of linearly crossing Dirac cone. Reproduced from Ref. [10].

for the recent development of topological materials, such as topological insulators [11], [12] and topological semimetals. Symmetry and symmetry breaking were thought to regulate phase transitions in condensed matter until the notion of topology was brought into condensed matter physics. The quantum Hall (QH) state, discovered in 1980 [9], provided the first example of a quantum state that has no spontaneously broken symmetry. Von

Klitzing *et. al.* discovered that when a two-dimensional (2D) semiconductor is exposed to a strong magnetic field, at very low temperatures, localization of electrons and Landau quantization of their energy spectrum lead the longitudinal resistance to become zero, while the Hall resistance exhibits quantized plateaus with heights of $h/\nu e^2$ [9], [13] provided the chemical potential is located in between Landau levels. Here, h is Planck's constant, ν is the filling factor, and e is the electron charge. This type of quantization of transport coefficients was recognized as macroscopic quantum phenomenon in Laughlin's gauge argument[5]. However the concept of quantization phenomenon was already established theoretically in 1974[14]. In 1982, Thouless, Kohmoto, Nightingale, and den Nijs (TKNN)[14] found that this phenomenon not only is quantum mechanical but also is topological. They also found that in the quantum Hall system the k-space is mapped to a topologically-nontrivial Hilbert space, whose topology can be specified by an integer topological invariant called TKNN invariant ν, later named Chern no, which is an integral invariant defined at the Brillouin zone and is unaffected by the system's geometry. This Chern number can be expressed by the integral of the Berry curvature in the 2D Brillouin zone-

$$\mathbf{C} = \frac{\mathbf{1}}{\mathbf{2\pi}} \int_{\mathbf{BZ}} \mathbf{d^2k}\ \boldsymbol{F_m}(\mathbf{K}) \qquad \textbf{(1.1)}$$

The Berry curvature $$\boldsymbol{F_m}(\mathbf{K}) = \Delta_k \times \boldsymbol{A_m}(\mathbf{K}) \qquad \textbf{(1.2)}$$

is the curl of the Berry connection of the *m*-th occupied band A_m. Figure 1.2 illustrates how IQHE can be stated semiclassically. Electrons move in cyclotron orbits when a magnetic field is applied, with their energy quantized as $\varepsilon_m = \omega_c(m + \frac{1}{2})$, where ω_c is the cyclotron frequency and m is an integer. These distinct energy levels, known as Landau levels, are degenerate and proportional to the strength of the magnetic field. Therefore, each Landau level can accommodate more electrons with rising magnetic field

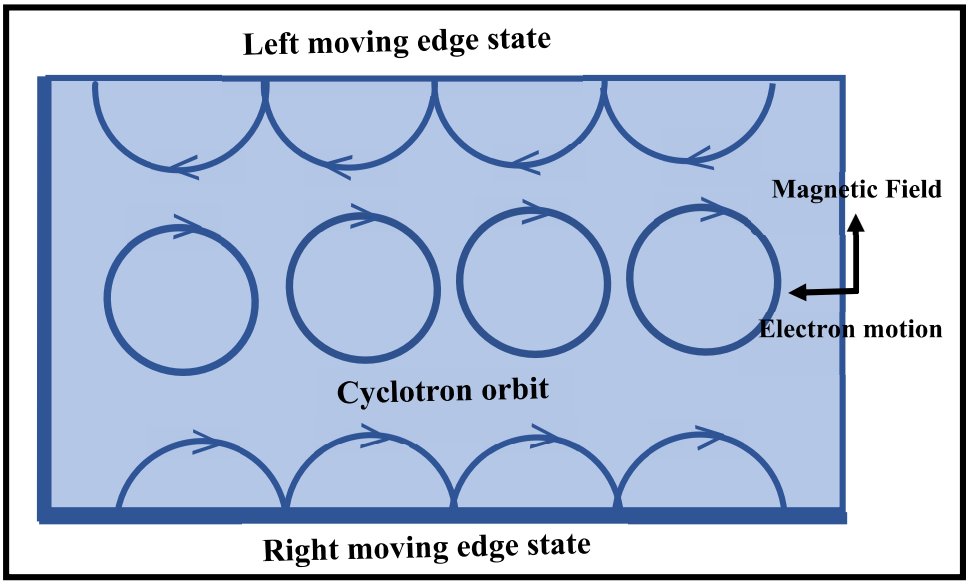

Figure 1.2 Semiclassical description of integer quantum Hall state.

To come into a stable state, electrons are forced to move from higher energy state to lower Landau level. If electrons occupy up to N^{th} Landau level, while the rest are empty, we observe a Hall conductivity,

$$\sigma_{xy} = Ne^2/h \tag{1.3}$$

In this configuration, Landau levels can be treated to be the energy bands as in band theory. So, with filled N^{th} Landau level separated from the empty $(N+1)^{th}$ level by a constant energy gap $\sim\hbar\omega_c$, integer quantum Hall state (IQHS) should behave like an ordinary insulator. Unlike an insulator, IQHS shows quantized Hall conductivity under an electric field. Another striking feature of IQHS is the presence of conducting edge states. They appear at the boundary of the 2D electron gas due to the skipping motion of electrons as their cyclotron orbits bounce off the edge. These states are called 'chiral' as they propagate to only one direction without backscattering irrespective of any disorder in the system. IQHE does not fit in the description of the conventional band theory of solids and paved the pathway to introduce the topological order in condensed matter physics.

The fractional quantum Hall (FQH) effect was discovered in 1982 by Tsui, Stormer, and Gossard[7]. In terms of topology, however, this doesn't have much connection to topological insulators.

1.2 Topology in geometry

Topology is a mathematical concept used to classify different geometrical objects [3]. In this framework, two objects are considered to be the same topological class if one can

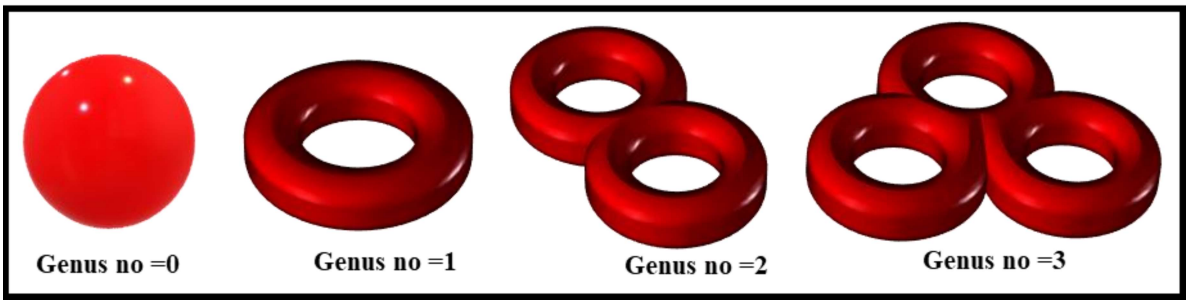

Figure 1.3 Geometrical objects with different topological classes represented by the genus numbers.

continuously deform into the other by stretching or bending without tearing or gluing. For example, a solid sphere can be turned into a disc by compressing along a diagonal axis. However, to a topologist, they are the same class of materials, just like a coffee mug can be transformed to a doughnut. So, a doughnut and a sphere are no longer a member of same group. One of the fundamental concepts in topology is to categorise objects by counting the number of holes they contain. To construct more formal definition, we use the value of genus (g) given by the Gauss-Bonnet theorem:

$$\int_{surface} K dS = 4\pi(1 - g), \qquad (1.4)$$

where K is the Gaussian curvature. For a sphere with radius r, $K = 1/r^2$ and Equation 1.4 leads to g = 0. In Figure 1.3, we have shown objects with different values of genus (same as the number of holes), representing different topological classes.

1.3 The concept of topology in integer quantum Hall effect

One cannot obtain an IQHS from a trivial insulator by smoothly varying the Hamiltonian as the topological invariant $\nu=0$ for a trivial insulator (such as vacuum), whereas IQHS is represented by $\nu = 1$. At some point, the band gap has to close, i.e., pass through zero to change the topological invariant. At this interface of trivial insulator (vacuum) and IQHS, the conducting chiral edge state appears as shown in Figure 1.4(a). The edge state is protected by the fundamental concept of topology and gives rise to a one-dimensional (1D) band dispersion in the bulk band gap [Figure 1.4(b)]. We can alter the dispersion of this 1D band by altering the Hamiltonian close to the surface. The number of left and right moving channels, or band dispersions that cross the Fermi level with a positive or negative group velocity, is fixed and specified by the bulk-boundary correspondence.

The Chern number can be used to determine whether a system is topologically trivial ($C = 0$) or nontrivial ($C > 0$) in 2D systems. Ordinary insulators have topologically equivalent energy bands to those of a vacuum, hence are topologically simple. There are, nevertheless, nontrivial topological systems that are topologically inequivalent to conventional insulators. Because of the different band topology, gapless edge states develop at the boundary between topologically nontrivial materials and ordinary insulators (vacuum) in 2D systems with broken time-reversal symmetry and $C \neq 0$. These edge states are known as chiral edge states because electrons can only travel unidirectionally along the boundary. Elastic backscattering by impurities is not allowed in these states. As a result, topological edge states can transport with little dissipation,potentially allowing for the development of next generation electronics and spintronics devices. Symmetry plays the crucial role in topological materials that are protected by certain symmetry, such as time-reversal symmetry, lattice symmetry, and electron–hole symmetry. The Chern number must be $C=0$ for materials with time-reversal symmetry.

1.4 The tour from quantum Hall to quantum spin Hall

The QH effect arises when a 2D electron gas in a semiconductor is subjected to strong magnetic field. At low temperature and high magnetic field, electrons travel through the edges and the two counterflows are spatially separated into different channels/lanes located at the sample's top and bottom edges.

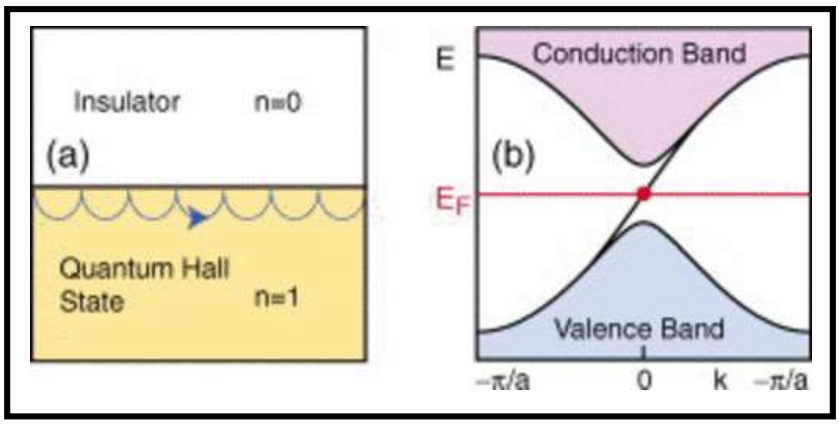

Figure 1.4 The interface between a quantum Hall state and an insulator has chiral edge mode. (a) The skipping cyclotron orbits. (b) The electronic structure of a semi-infinite strip described by the Haldane model. A single edge state connects the valence band to the conduction band. Reproduced from Ref. [15].

In a 1D system, electrons propagate in both the directions, in contrast the top edge of a QH bar carries only half the degrees of freedom (DOF). That spatial separation is the main reason why the QH states are topologically robust. When such an edge-state electron encounters an impurity, it simply takes a detour and still continue its flow as there is no scope for turn back. This gives QH state a unique platform to achieve dissipationless current flow. However, in a spinful 1D system there are 4 channels- spin-up forward mover [Figure 1.5(a) and (b)], spin-down backward mover on the top edge and the other two channels on the bottom edge. This is called quantum spin hall (QSH) state as it contains a net transport of spin forward along the top edge and backward along the bottom edge, just like the separated transport of charge in the QH state. In the quest for such QSH state, F. D. M.

Haldane, B. A. Bernevig and S.-C. Zhang predicted that spin-orbit coupling (SOC) can play

Subsequently, they (B. A. Bernevig, T. L. Hughes, S.-C. Zhang) also predicted that such

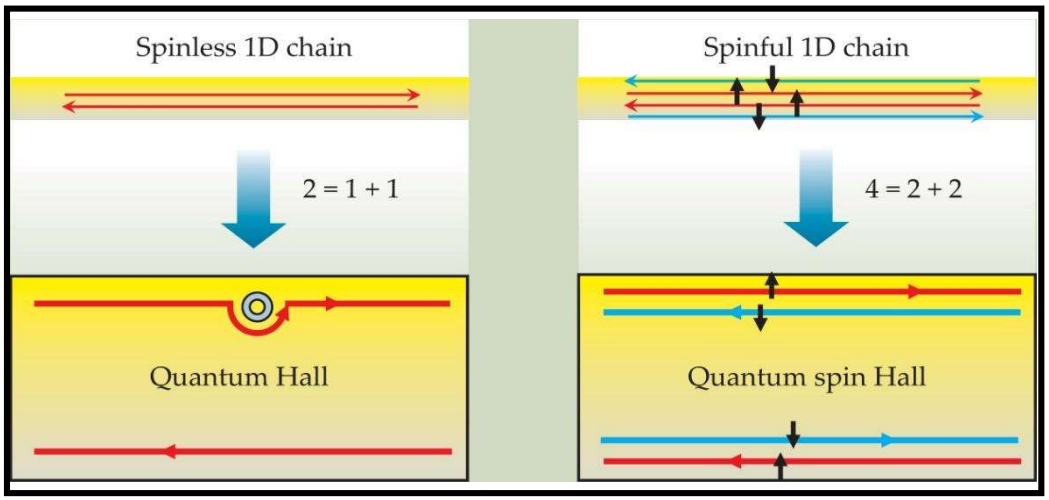

Figure 1.5 Spatial separation is at the heart of both the quantum Hall (QH) and the quantum spin Hall (QSH) effects. (a) A spinless one-dimensional system has both a forward and a backward mover. Those two basic degrees of freedom are spatially separated in a QH bar, as illustrated by the symbolic equation "2 = 1 + 1." The upper edge contains only a forward mover and the lower edge has only a backward mover. The states are robust: They will go around an impurity without scattering. (b) A spinful 1D system has four basic channels, which are spatially separated in a QSH bar: The upper edge contains a forward mover with up spin and a backward mover with down spin, and conversely for the lower edge. That separation is illustrated by the symbolic equation "4 = 2 + 2." Reproduced from Ref. [16].

state can be observed in HgTe/CdTe quantum well, which was experimentally realized by L. W. Molenkamp and his collaborators in 2007. This is the first discovery of a 2D topological insulator (TI) or quantum spin Hall insulator (QSHI). The edge states must have an odd number of backward movers and an odd number of forward movers for the QSH state to be robust. The core of the QSH state is the even-odd effect, which is represented by a Z_2 topological quantum number. Thus, a QSH insulator is also referred to as a topological insulator. A QSHI can be conceptualized as the superposition of two IQHSs with opposing chiral edge channels. Depending on the direction of the intrinsic magnetic field produced by the SOC, each edge channel has a single spin state associated with it, either spin-up or spin-down, and it propagates either clockwise or anticlockwise. This unique state preserves time reversal symmetry (TRS). From band dispersion perspective,

these edge states represent two 1D bands in the bulk band gap intersecting the Fermi energy, one with positive and another with negative group velocity. These two bands merge at TRS invariant momenta k = 0 and π/a (same as -π/a; a is the lattice parameter). Generally, band crossing leads to hybridization and opening of gap at the crossing point. But, in the present situation, two bands cannot hybridize as they are preserved by the TRS protection. Kramer's theorem says, the band crossing points must be doubly degenerate under TRS. The edge states are of a TI are very robust, independent of disruptions and impurities. Kane and Mele[17], [18] classified time-reversal invariant system by another type of topological invariant known as the Z_2 invariant. Here, the index Z_2 can take only two values, i.e., 0 or 1, depending on the parity of the intersection numbers between the edge states and the Fermi level. As a result, 2D time-reversal invariant insulators can be classified into two groups: topologically trivial insulators with Z_2 invariant equal to 0 are topologically trivial, with edge states intersecting with the Fermi level an even number of times, and topological insulators with Z_2 invariant equal to 1 are topological insulators (TI), with edge states intersecting with the Fermi level an odd number of times and always existing in the bulk gap[15], [17], [18]. Figure 1.6(a)-(d) represents the edge/surface states in TI with Dirac dispersion. Among them, HgTe/CdTe quantum wells[19], InAs/GaSb quantum wells[20] are 2D TIs. The edge states of a 2D TI, also known as helical states, are made up of a pair of counter-propagating chiral states with spin-momentum locking, in which electrons travelling in opposite directions have opposite spins; this feature is due to time-reversal symmetry, which prevents electron backscattering. When the bulk state is insulating, the helical states contribute the majority of the transport signal, resulting in the so-called quantum spin Hall effect (QSHE)[17], [18], [21]. The quantized longitudinal resistance has been observed in HgTe/CdTe quantum wells[21], InAs/GaSb quantum well[20] and also in monolayer WTe_2[23] as an evidence of QSHE transport in 2D TI. However, the

longitudinal-resistance plateau in 2D TIs, on the other hand, is imperfect, and certain findings contradict theoretical predictions[24]. In 3D, the TIs are identified by four Z_2

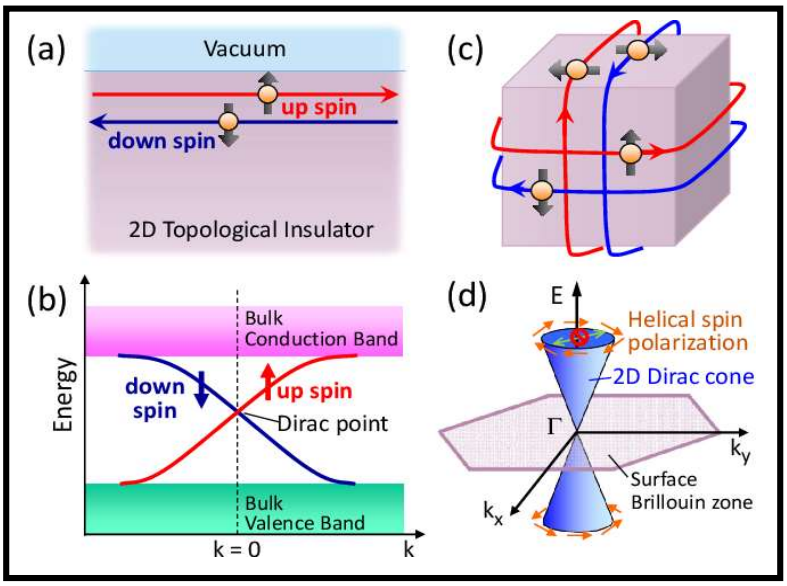

Figure 1.6 (Color online) Edge and surface states of topological insulators with Dirac dispersions. (a) Schematic real-space picture of the 1D helical edge state of a 2D TI. (b) Energy dispersion of the spin non-degenerate edge state of a 2D TI forming a 1D Dirac cone. (c) Schematic real-space picture of the 2D helical surface state of a 3D TI. (d) Energy dispersion of the spin non-degenerate surface state of a 3D TI forming a 2D Dirac cone; due to the helical spin polarization, back scattering from k to -k is prohibited. Reproduced from Ref. [22].

topological invariants ($\nu_0;\nu_1\nu_2\nu_3$). Accordingly, the TIs can be further classified as "strong TI" and "weak TI". While the ν_0 index is nontrivial for strong TI, which are characterized by metallic surface states forming an odd number of Dirac cones. These states are robust against perturbations that do not break the time-reversal symmetry. The ν_0 index becomes vanishing but ($\nu_1\nu_2\nu_3$) indexes are nontrivial for weak TIs. At present, the most representative strong TIs are materials are Bi_2Te_3 family[25] and recently in $ZrTe_5$[26], in contrast, weak TI are [27].

1.5 Topological Insulator to Topological Semimetals (TSMs)

The discovery of a topological insulator invigorates significant scientific attention in searching for nontrivial states in semimetallic and metallic materials. This finally leads to

the observation of the nontrivial state in the zero-bandgap system unlike the gapped system in TI. Semimetals are widely recognized for having a small or vanishing density of states near the Fermi energy (E_F). They include materials in which the finite density of states is induced by the crossing or touching of conduction and valence bands in the three-dimensional (3D) Brillouin zone (BZ). Such band crossings are usually associated with a topological invariant and result in a topological phase change[28]. Therefore, topological semimetal is a new gapless material with topologically protected Dirac cones. They exhibit novel macroscopic quantum phenomena that are not only of fundamental interest, but may also possess technological implications.

The field of TSMs is now emerging at lightining speed. This is due to theoretical and experimental advancement of relativistic particle discovered[11], [29]–[32]. While the majority of TSMs found so far are known compounds, their topological nature was unclear for many years. Specifically, the experimental realization of both Weyl and Dirac semimetals has propelled the field to the forefront of quantum condensed-matter research in last few years. Nodal-line semimetals, two-, three-, four-, six- and eight-fold semimetals are other kinds of experimentally identified semimetals so far depending on the nature of band crossing points. According to the dimensionality of the band crossings, these TSMs can be categorized into following types- i) the zero-dimensional (0D) band crossings are well known as nodes or nodal points. In the case of Dirac semimetals (DSMs) and Weyl semimetals (WSMs), two doubly or singly degenerate bands cross each other at discrete points near E_F generating fourfold Dirac points or twofold Weyl points, researchers also predicted many other types of nodal points called type-II nodal points, threefold, sixfold, and eightfold degenerate nodal points [34]–[37], ii) this group contains-fourfold or twofold band crossings along one-dimensional (1D) lines in the momentum space. Materials with such nodal lines are called topological nodal-line semimetals (TNLSMs), TNLSMs, like

WSMs, have distinct surface states known as drumhead surface states, which are characterised by flat surface bands embedded inside the surface projection of the bulk nodal lines[38]. The schematic of DSM, WSM, NDSM is manifested in Figure 1.7.

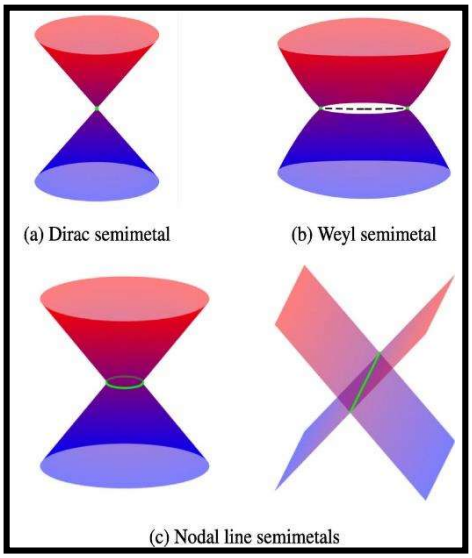

Figure 1.7 Schematic illustration of Dirac node, Weyl node and Nodal line/ ring in momentum space. (a) Schematic of a Dirac semimetal where the bands are linearly dispersed around the Dirac point. The Dirac point is shown by the green dot. (b) Weyl semimetal, in which the Weyl points with opposite chirality are connected by the characteristic Fermi arc. The Weyl points are shown by the green dot and Fermi arc is shown by the black dotted line. (c) Nodal line semimetals where valence and conduction bands cross along special lines in momentum space forming either a ring-shaped line or 1D line, shown by the green circle/line. Reproduced from Ref. [33].

The surface states of the drumhead, on the other hand, are not topologically protected, and even a minor perturbation can ruin the flatness of the surface bands[11]. iii) new sort of band crossing that is preserved in a 2D surface in the 3D BZ. Nodal-surface semimetals [39], [40] have received less attention than Dirac, Weyl, and nodal-line semimetals. Only a few nodal-surface semimetals have been predicted so far, and the nodal surface has only recently been discovered in the ZrSiS family of materials[41].

1.5.1 Weyl Semimetals (WSMs)

In 1929, Hermann Weyl demonstrated the existence of a massless fermion in the Dirac equation [42], which was later called the Weyl fermion. In the standard model, all fermions are Dirac fermions, except neutrinos that possess chirality. Weyl Fermions exist as a low-energy excitations in Weyl semimetal in which electronic bands disperse linearly along the three-dimensional momentum space from a node called a Weyl point. WSMs are associated with the lack of time-reversal or inversion symmetry. These Weyl points act as topological charges that means as sources (+ chirality) and sink (- chirality) of Berry curvature. The Berry curvature is a quantity that can characterize the topological entanglement between conduction and valence bands, which is equivalent to a magnetic field in the momentum space. These Weyl points always appear in pairs[43], [44]; otherwise, the Berry flux becomes divergent. WSMs are divided into two categories: The linear nondegenerate bands cross at the Weyl points (WPs) in type-I WSMs, resulting in a point like Fermi surface (FS) if the chemical potential is tuned to the energy of WPs; however, in type-II WSMs, the Lorentz symmetry is broken, and the hole and electron pockets, which form the WPs, overlap over a range of energies, resulting in a finite density of states. The existence of non-conservation of chiral charge caused by parallel electric and magnetic fields is one of the most distinctive aspects of WSMs. The band structure of a WSM originates from the band inversion in proximity to a TI[42]. The existence of non-conservation of chiral charge caused by parallel electric and magnetic fields is one of the most distinctive aspects of WSMs[45], [46]. In this situation, the generation of the electric current or the negative magnetoresistance (MR) can be realized in the presence of parallel electric and magnetic fields. Another important aspect of these semimetal are the unique open Fermi surfaces called Fermi arc. This Fermi arc is an unclosed line that starts from one Weyl point and ends at the other with opposite chirality [Figure 1.8(a)] and verified by surface-sensitive

technique- angle-resolved photoemission spectroscopy (ARPES). WSMs have been predicted in pyrochlore iridates $Y_2Ir_2O_7$ [47], $HgCr_2Se_4$ [48], and $Hg_{1-x-y}Cd_xMn_yTe$[50], however, not experimentally realized so far except for the candidates- $K_2Mn_3(AsO_4)_3$[51] and magnetic Weyl semimetal $Co_3Sn_2S_2$[52].The type-I WSMs are -TaAs, NbAs, NbP, TaP[53], [54], characterized by pairs of linearly dispersing touching points between the valence and the conduction bands, in contrast the type-II WSMs result from linear touching

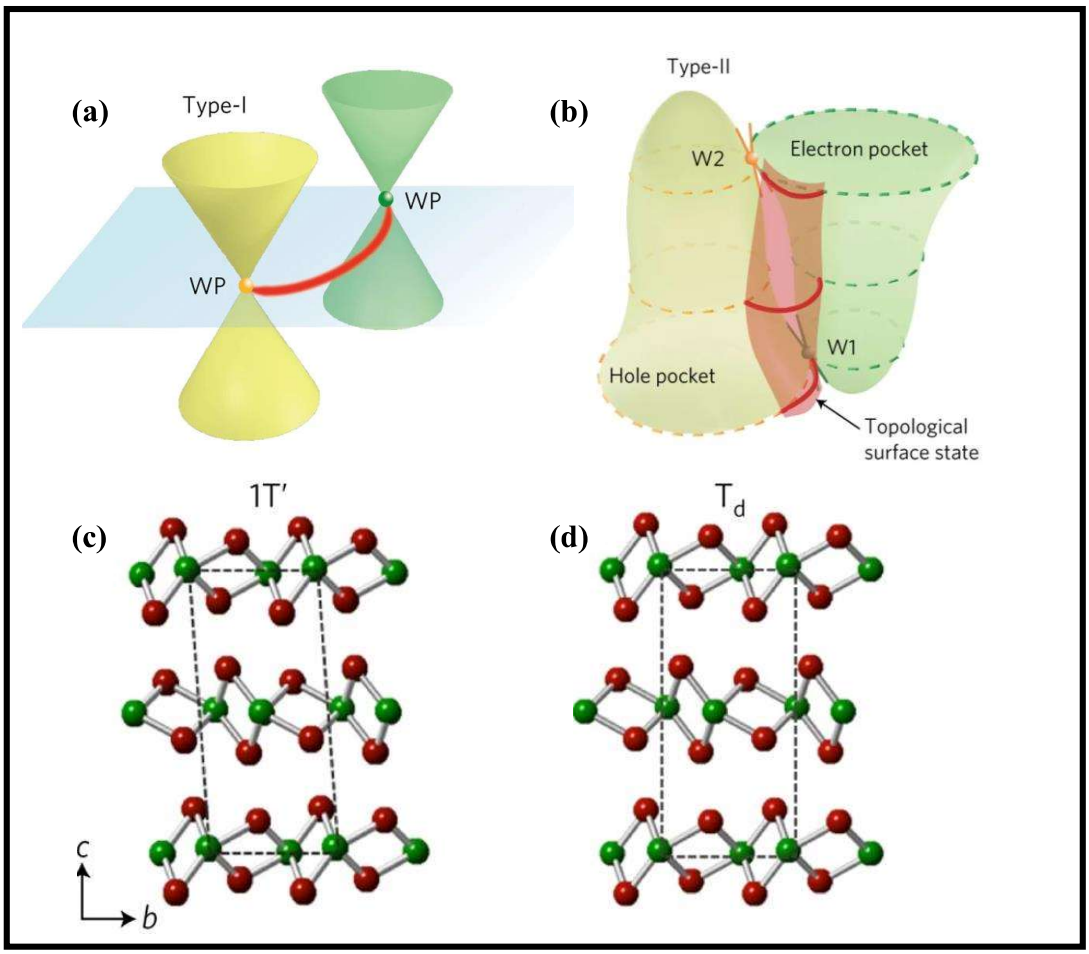

Figure 1.8 (a) Dispersions for type-I Weyl fermion near E_F. The Weyl points (WP) are labelled by yellow and green dots, (b) Type-II Weyl semimetal with electron and hole pockets touching at two different energies, Crystal structures of $MoTe_2$ (c) in the 1T′ and in (d)T_d phases. Reproduced from Ref. [49].

points at the boundary between electron and hole pockets [Figure 1.8(b)]. Various candidates of type-II WSMs are- $MoTe_2$, WTe_2 and their derivatives $W_{1-x}Mo_xTe_2$[55]–[58].

Another type-II candidate is $NbIrTe_4$[59]. Type-II WSMs have different properties than type-I WSMs, such as an anisotropic chiral anomaly that changes depending on the current direction and unique AHE[55]. Furthermore, the layered structure of these compounds makes device fabrication easier, making them a potential platform for developing innovative WSM applications. Among the type-II WSMs, T_d-phase of $MoTe_2$ has attracted much attention due to their XMR property, perfect electron-hole compensation and turn-on phenomenon[60]. $MoTe_2$ crystallizes in several phases- semiconducting 2H phase, 1T′ and T_d-phase. The 2H phase (α-phase) is semiconducting with the Mo atoms being trigonal-prismatically coordinated by Te atoms forming stacked layers which couple through a weak, or a van der Waals–like interaction. Both 1T′ (β phase) and T_d phases (γ-phase) show semi-metallic nature. The noncentrosymmetric T_d phase (orthorhombic and no inversion symmetry) is achieved on cooling the centrosymmetric 1T′ (monoclinic) phase at 240K[61], [62]. The 1T′ and T_d-phases of $MoTe_2$ is shown in Figure 1.8(c) and (d). WTe_2 is known to crystallize only in an orthorhombic T_d-phase similar to γ-phase of $MoTe_2$.

The electron and hole pockets touch each other at 6 meV (labeled as W1) and 59 meV (labeled as W2) above E_F, forming four pairs of type-II Weyl points with monopole charges of ±1, as illustrated in Figure 1.9(a) and (b) depicts the estimated electronic band structure of $MoTe_2$ in the presence of SOC in the k_z =0 plane along a specific K-K′ direction. Topological Fermi arcs are expected to arise on the 001 surface, connecting the opposing chirality projections of the W1 and W2 Weyl points, as illustrated in Figure 1.9 (c). Surface Fermi arcs are difficult to differentiate from trivial surface states or projected bulk states experimentally because they are both squeezed into the narrow surface gap between the projected bulk electron and hole pockets [Figure 1.9 (d)]. A topological Fermi

arc above E_F has been shown in Figure 1.9 (f) and (g) for the type-2 Weyl semimetal $Mo_{0.25}W_{0.75}Te_2$.

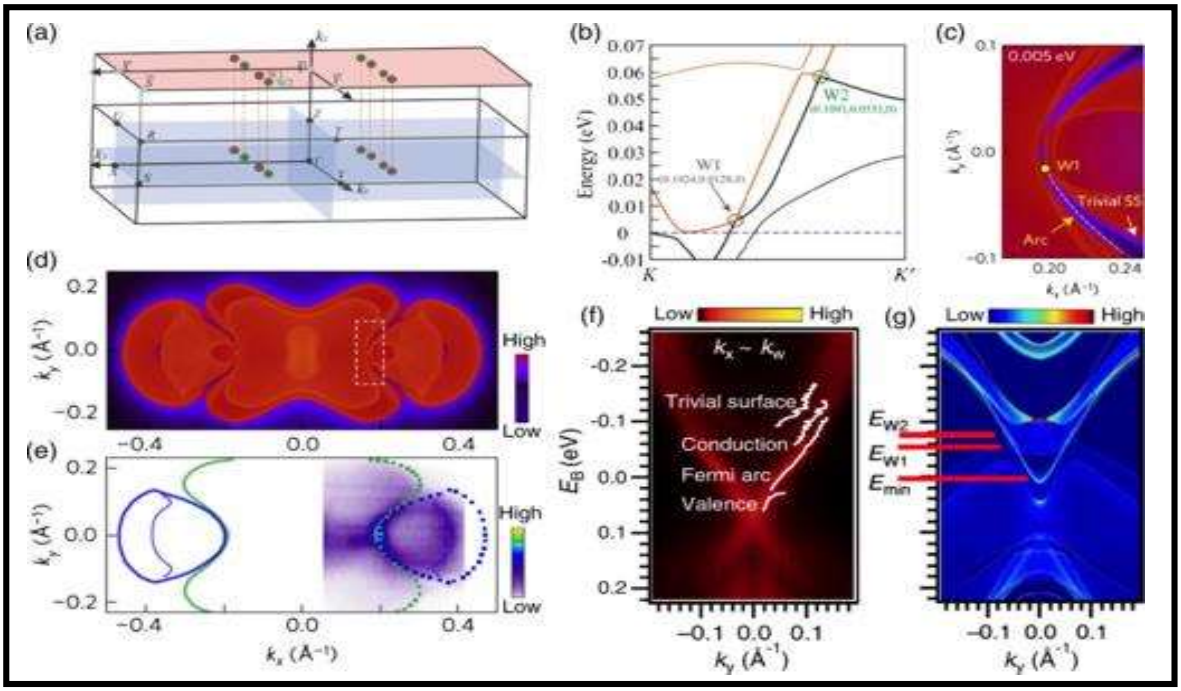

Figure 1.9 (a) 3D bulk BZ and the projected (001) surface BZ of $MoTe_2$. Weyl points with positive and negative monopole charges are displayed as green and gray dots. (b) Calculated fine band structure of $MoTe_2$ along the K-K′ direction crossing two types of Weyl points. (c) Calculated spectral intensity maps of $MoTe_2$ at E_F +5 meV. (d) Calculated spectral intensity maps of $MoTe_2$ at E_F (shifted by −0.02 eV to account for the slight hole doping). The white dashed boxes indicate the regions of interest shown in (c). (e) ARPES intensity maps of $MoTe_2$ measured at E_F with a 6.3 eV laser. (f), (g) ARPES intensity plot and the calculated electronic structure of $Mo_{0.25}W_{0.75}Te_2$ at kx ~ kw along the ky direction. The red lines indicate the energy positions of the surface band bottom, the W1 point, and the W2 point, respectively. Reproduced from Ref. [63].

1.6 Magnetic Topological Materials

The anomalous Hall effect (AHE) measurement has emerged as a potent technique for studying magnetic materials such as ferromagnetic metals, magnetic semiconductors, and magnetic topological insulators in great detail. The AHE is a fundamental transport property of magnetic materials in which the interaction of magnetism and spin-orbit coupling creates a transverse Hall voltage perpendicular to the applied current and the magnetization[64], [65]. Magnetically doped three-dimensional topological insulators have

recently provided an ideal platform to discern the AH effect and its connection to band topology. The topological insulator hosts time reversal symmetry protected surface state in which the spins of the Dirac electrons are locked perpendicular to their momenta direction. TI, when doped with magnetic impurities, large variety of magnetic phases, such as ferromagnetic, paramagnetic, noncolinear, and spin glass phases, emerging from various types of exchange interactions between the magnetic impurities in presence of the surface and bulk states[66]–[69]. The Hall resistivity in ferromagnetic material can be written as $\rho_{xy} = \rho^0+\rho^{AH}$, where ρ^0 is ordinary Hall contribution ($\rho^0= R_OB$, where, R_O is the ordinary Hall coefficient, B is the magnetic field) and ρ^{AH} is the AHE contribution, which comes from the magnetization of the material ($\rho^{AH} = R_{AH}M$, where R_{AH} is AH coefficient, and M is magnetization of material). The first term describes the ordinary Hall effect and caused by the Lorentz force acting on moving charged carriers, whereas the origin of the second term has been a controversial topic for many years. To explain the origin of AHE two possible mechanisms have been proposed. An extrinsic mechanism includes skew scattering and side jump which relates the scattering events, another one is an intrinsic mechanism related to the band topology of the system[65], [70], [71]. In 1954, Karplus and Luttinger proposed the intrinsic mechanism (K-L theory), which is connected to the role of SOC in ferromagnetic material's electronic band structure and leads to anomalous electron velocity perpendicular to the electric field direction. Later this theory was explained by Berry phase and Berry curvature. As we are aware that the, the Berry curvature is equivalent to a fictional magnetic field in momentum space connected to the geometrical phase of the electronic wave function, the transverse momentum of the electrons is introduced via Berry curvature in momentum space, resulting in intrinsic AHE[72], [73]. On the other hand, skew scattering is the asymmetric scattering which is caused by the effective spin-orbit coupling of the electron or the impurity. Additionally, side jump mechanism comes into

play when the electron velocity is deflected in opposite directions by the opposite electric fields experienced upon approaching and leaving an impurity[65]. The Anomalous Hall conductivity σ_{xy} varies linearly ($\sigma^{A}_{xy} \propto \sigma_{xx}$) with longitudinal conductivity, σ_{xx} for a skew scattering case, however if it varies quadratically ($\sigma^{A}_{xy} \propto \sigma_{xx}^{2}$), the origin is due to intrinsic Berry curvature or skew scattering[65], [74]. The longitudinal conductivity (σ_{xx}) and the Hall conductivity (σ^{A}_{xy}) were calculated using following relation-

$$\sigma_{xx} = \frac{\rho_{xx}\,(B=0)}{\rho_{xx}^{2}\,(B=0) + \rho_{xy}^{2}} \quad \text{and} \tag{1.5}$$

$$\sigma_{xy}{}^{A} = \frac{\rho^{A}{}_{yx}}{\rho_{xx}^{2}\,(B=0) + (\rho^{A}{}_{yx})^{2}} \tag{1.6}$$

Here, ρ_{xx} and ρ_{yx} are the longitudinal and Hall resistivity, respectively. Again, the contribution of side jump in AHC can be expressed as $\frac{e^{2}\varepsilon_{SO}}{haE_{F}}$, where ε_{so} is the spin–orbit interaction and the term ε_{so}/E_F is order of 10^{-2} for the most of the ferromagnetic metals, so negligible compared to the intrinsic contribution, E_F is Fermi energy[75], [76]. The terms e, h and a are the electronic charge, Planck constant and lattice parameter, respectively. However, it is not possible to separate the intrinsic contribution from the side jump mechanism practically because both have similar dependencies on σ_{xx}. In many Co-based Heusler based materials Co_2FeAl (T_c~810-900K)[77], $Co_3Sn_{2-x}In_xS_2$ (T_c~176K)[78] and Kagome lattices $GdMn_6Sn_6$ (T_c~440K)[79], YMn_6Sn_6 (T_N~359K)[80], $LiMn_6Sn_6$ (T_C=382K)[81], $HoMn_6Sn_6$ (T_c~383K) and $DyMn_6Sn_6$ (T_c~398K)[82], $TbMn_6Sn_6$ (T_C = 423 K)[83], the AHC was explained by the connection of Berry curvature and electronic band structure. The AHC and longitudinal conductivity are of the order of ~10^2-10^3 $\Omega^{-1}cm^{-1}$ in all these compounds. Three broad regimes can be identified based on the values of longitudinal conductivities: (i) a high conductivity regime where $\sigma_{xx} > 10^6$ $\Omega^{-1}cm^{-1}$ in which $\sigma^{A}_{xy} \propto \sigma_{xx}$ that means skew scattering dominates, (ii) σ_{xx} ~ 10^4-10^6 $\Omega^{-1}cm^{-1}$

where σ_{xy} =const. the regime of intrinsic or scattering independent region; and (iii) $\sigma_{xx} < 10^4$ $\Omega^{-1}cm^{-1}$ is called dirty or bad metal region where $\sigma^A_{xy} \propto \sigma^{1.6}_{xx}$ is predicted[65]. In the region of skew-scattering the anomalous Hall ratio $\sigma_{xy} / \sigma_{xx} \sim \tan\theta$ is small ~ 0.1–1% because the spin–orbit interaction is usually smaller than the width of the virtual bound state and also skew-scattering requires the phase shifts of different orbital angular momenta[71], [84], [85]. Interestingly, when the Hall angle is large ~ 0.1π rad and σ_{xy}, σ_{xx} are quite larger compared to the typical scattering value then spin-chirality enhanced skew scattering is considered. This spin chirality or the noncoplanar spin structure comes from the triangular spin cluster/ tilted magnetic cluster systems[86]. This type of spin arrangements is common in Kagome net and act like a "compound magnetic scattering center", when an external field is applied. A distortion between the local order results in a net magnetization and magnetic fluctuations act as scattering centers generating an enhanced skew scattering potential[87]. When compared to the energy scale of the hybridization between the resonance state and the conduction electrons, this spin-orbit interaction is regarded to constitute a weak disruption in a typical ferromagnet. As a result, the scattering skew angle is quite small, leading to small AHE. The skew scattering by many scatterers, on the other hand, is not limited in this way. AHE is strongly related to the scalar spin chirality of impurity spins [88]. Scattering by multiple magnetic scatterers also adds to AHE. The skew scattering connected to the three-spin scattering further revealed that this AHE is an extrinsic AHE[89], [90]. Furthermore, in some situations, a mechanism related to vector spin chirality contributes to the AHE [90]–[92]. So far, these investigations have focused on the weak-coupling limit, where impurities are considered as perturbations; studies on such phenomena in the strong-coupling situations have been limited to these works [92]–[94]. Strong-coupling events, on the other hand, are observed experimentally in transition-

metal materials [95], [96]. Very few works have reported on multiple spin scatterer problem where the electron-spin interaction is high.

As the intrinsic mechanism is a consequence of the Berry curvature of the electronic bands as a result of SOC, a similar phenomenon occurs from spin Berry phase as an effect of "spin chirality" of neighboring spins. The scalar spin chirality is a quantity in magnetism that characterizes the noncoplanar structures of spins, such as in antiferromagnets[97] and spin glasses[98], [99], and it is related to a topological number that characterizes the spin texture[100] when long range ordering is there. Scalar spin chirality defined by $S1 \cdot S2 \times S3$, where $Si = (S_i^x, S_i^y, S_i^z$ $(i = 1, 2, 3)$ is the three adjacent spins. Skew scattering can be developed by this spin chirality and results into enhanced skew scattering. Interestingly, this AHE can survive even above the magnetic ordering temperature indicating thermal average of the spin chirality, in contrast, the intrinsic AHE based on the intrinsic Berry phase disappears above the ordering temperature. AHE above the magnetic ordering temperature has been observed in many skyrmions[101], [102], originating from skew scattering of fluctuating but locally correlated spins. In addition, large AHE related to the spin cluster scattering has been observed in a Kagome metal even without magnetic ordering[86]. Researchers also found that the anomalous Hall angles increase with decrease in charge carriers and increase with exchange coupling between the localized spins[87]. Other than spin chirality contribution towards skew scattering, magnetic and thermal fluctuations are also responsible for large AHC[86], [102].

1.6.1 Quantum oscillations

We know that the electrons moving in a strong transverse magnetic field, undergo cyclotron motion. Their energy states then become quantized and form Landau levels. With increasing magnetic field strength, the degeneracy of each Landau level increases and electrons are pushed to lower Landau levels to minimize the energy. When an upper Landau

level becomes empty, i.e., Fermi energy of the system passes through the Landau level, it is reflected as oscillation of the physical quantities such as resistivity (Shubnikov-de Haas effect), magnetization (de Haas-van Alphen effect), thermoelectric power etc. The frequency of these oscillations, also known as quantum oscillations, is proportional to the extremal Fermi surface cross-sectional area perpendicular to the direction of the applied magnetic field. Hence, by probing the quantum oscillation along different crystallographic directions, we can construct the complete Fermi surface of any material. In addition, from the magnetic field and temperature dependence of the oscillation amplitude, several Fermi surface related parameters can be calculated.

1.7 Topological insulator under pressure

Apart from the various effects of magnetism on electronic bands of topological insulators, TIs are very interesting to explore under extreme pressure. High-pressure studies are very beneficial for understanding and tuning the materials properties that allows us to reduce the interatomic distances and to utilize in many applications. For example, when an extreme of the electronic-band structure, related to the Van Hove singularity in the density of states, crosses the Fermi energy level, it is called an ETT or Lifshitz transition and occurred under the application of pressure. Pressure, temperature, doping, and other factors can cause a change in the topology of the Fermi surface, which modifies the electronic density of states around the Fermi energy. As ETT is a 2.5 transition in the Ehrenfest definition of phase transitions, no discontinuity in volume (first derivative of the Gibbs free energy) is expected in the neighbourhood of the ETT, but a change in compressibility (second derivative of the Gibbs free energy) is expected. It is also important to mention that the change of the topology of the Fermi surface is not connected with a change in the symmetry of the lattice, and therefore does not correspond to a phase transition of second order[103]. Another important phenomenon related to the ETT is topological quantum phase transition or TQPT

[104] where the topological index Z_2 undergoes a change from (0; 000 trivial) to (1; 000 nontrivial) under pressure and a topic of great scientific interests. When some of the trivial SOC narrow band gap materials at ambient temperature transformed into a nontrivial topological insulator by applying strain, the former comes into picture. It is an isostructural second-order transition which arises as a consequence of an adiabatic band inversion occurring at the time reversal invariant momenta point (TRIM) with parity change (odd/even). In this process, the topological invariant Z_2 changes from $Z_2 = 0$ (conventional insulator) to $Z_2 = 1$ (topological insulator) or vice versa. In general, strain can be induced into the SOC materials by either chemical or physical routes. Some other important aspects of pressure dependent studies are metal-insulator transition[105], and superconductivity[106]. Crystal structure will be compressed when the pressure is applied. Therefore, crystal level splitting is improved, and the bulk energy gap between the top of the valence band and the bottom of the conduction band at the point shrinks. The valence band and the conduction band will cross to generate a semimetallic/metallic state if the pressure is high enough.

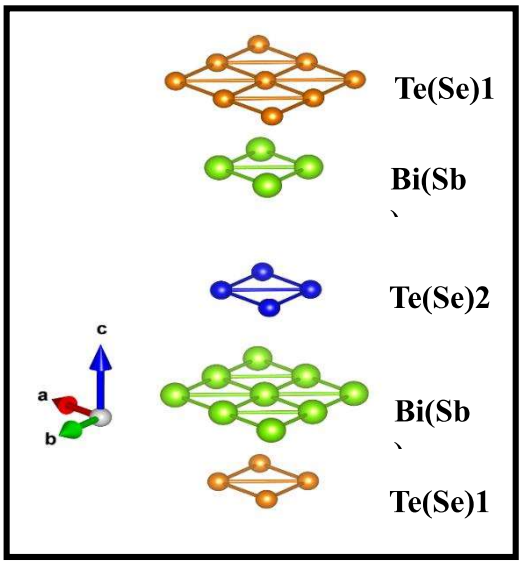

Figure 1.10 Five mono atomic planes of a quintuple layer of Bi_2Te_3/Sb_2Te_3.

1.7.1 Crystal Structure and symmetry properties under pressure

Narrow bandgap semiconductor Bi_2Te_3/ Sb_2Te_3/ Bi_2Se_3 has a tetradymite crystal structure [R-3m, S.G. 166, no of atoms per unit cell Z = 3]. This rhombohedral-layered structure is formed by layers. Figure 1.10 shows the 5 atomic planes of a quintuple layer of a Topological insulator with rhombohedral structure. This consist of five hexagonal close-packed atomic sublayers Te1/Se1-Bi/Sb-Te2/Se2-Bi/Sb-Te1/Se1, called quintuple layers and connected by weak van der Waals forces. The same layered structure is common to narrow bandgap semiconductor chalcogenides, like Bi_2Se_3 and Sb_2Te_3. The rhombohedral (R-3m) structure (α-phase) is found to transform into C2/m (β-phase, S.G. 12, Z = 4) and the C2/c (γ -phase, S.G. 15, Z = 4) transforms to a disordered bcc structure Im-3m structure, (δ-phase, S.G. 229, Z = 1) under the high pressure. Figure 1.11 represents the schematic of various structures under the application of pressure.

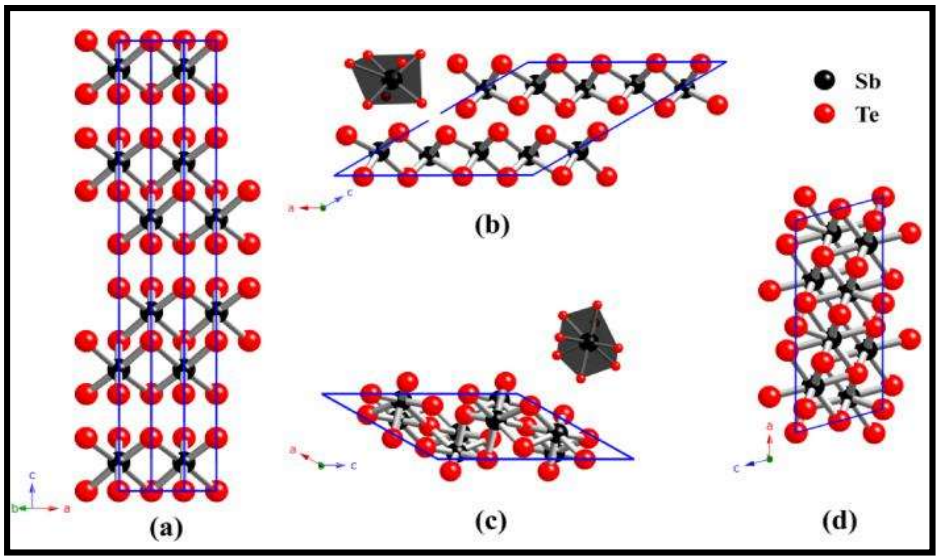

Figure 1.11 Schematic crystal structures of Sb_2Te_3 polymorphs: (a) α-Sb_2Te_3; (b) β-Sb_2Te_3; (c) γ -Sb_2Te_3 and (d) δ-Sb_2Te_3. Reproduced from Ref. [107].